Monthly Notices
of the
ROYAL ASTRONOMICAL SOCIETY

MNRAS **467,** 4763–4776 (2017)
Advance Access publication 2017 February 8

doi:10.1093/mnras/stx333

A multiwavelength continuum characterization of high-redshift broad absorption line quasars

D. Tuccillo,[1,2]★ G. Bruni,[3]★ M. A. DiPompeo,[4,5] M. S. Brotherton,[5] A. Pasetto,[3] A. Kraus,[3] J. I. González-Serrano[2] and K.-H. Mack[6]

[1]*GEPI, Observatoire de, CNRS, Université Diderot, 61, Avenue de l'Observatoire, F-75014 Paris, France*
[2]*Instituto de Física de Cantabria (CSIC-Universidad de Cantabria), Avda. de los Castros s/n, E-39005 Santander, Spain*
[3]*Max Planck Institute for Radio Astronomy, Auf dem Huegel, 69, D-53121 Bonn, Germany*
[4]*Department of Physics and Astronomy, Dartmouth College, 6127 Wilder Laboratory, Hanover, NH 03755, USA*
[5]*Dep. of Physics and Astronomy 3905, University of Wyoming, 1000 East University, Laramie, WY 82071, USA*
[6]*INAF-Istituto di Radioastronomia, via Piero Gobetti, 101, I-40129 Bologna, Italy*

Accepted 2017 February 6. Received 2017 February 6; in original form 2016 July 25

ABSTRACT

We present the results of a multiwavelength study of a sample of high-redshift radio-loud (RL) broad absorption line (BAL) quasars. This way, we extend to higher redshift previous studies on the radio properties and broad-band optical colours of these objects. We have selected a sample of 22 RL BAL quasars with $3.6 \leq z \leq 4.8$ cross-correlating the FIRST radio survey with the Sloan Digital Sky Survey (SDSS). Flux densities between 1.25 and 9.5 GHz have been collected with the Jansky Very Large Array and Effelsberg-100 m telescopes for 15 BAL and 14 non-BAL quasars used as a comparison sample. We determine the synchrotron peak frequency, constraining their age. A large number of gigahertz peaked spectrum and high-frequency peakers sources have been found in both samples (80 per cent for BAL and 71 per cent for non-BAL quasars), not suggesting a younger age for BAL quasars. The spectral index distribution provides information about the orientation of these sources, and we find statistically similar distributions for the BAL and non-BAL quasars in contrast to work done on lower redshift samples. Our sample may be too small to convincingly find the same effect, or might represent a real evolutionary effect based on the large fraction of young sources. We also study the properties of broad-band colours in both optical (SDSS) and near- and mid-infrared (UK Infrared Telescope Deep Sky Survey and *Wide-field Infrared Survey Explorer – WISE*) bands, finding that also at high-redshift BAL quasars tend to be optically redder than non-BAL quasars. However, these differences are no more evident at longer wavelength, when comparing colours of the two samples by mean of the *WISE* survey.

Key words: methods: data analysis – galaxies: active – galaxies: high-redshift – quasars: absorption lines – quasars: general.

1 INTRODUCTION

Intrinsic absorption lines are a common feature in quasar (QSO) spectra, and they are likely produced by outflowing winds along the line of sight that are launched from the accretion disc around the central supermassive black hole (Murray et al. 1995; Proga, Stone & Kallman 2000). Broad absorption lines (BALs) in ultraviolet and visible spectra of quasars are the most spectacular manifestation of such outflows, with absorption velocity width larger than 2000 km s^{-1} (Weymann et al. 1991). BAL QSOs are often classified into three subtypes depending on the presence of absorption lines in specified transitions: (1) High-ionization (Hi) BAL QSOs show absorption lines in high-ionization transitions such as Si IV and C IV; (2) Low-ionization (Lo) BAL QSOs possess Mg II and/or Al III absorption lines, in addition to the high-ionization transitions. (3) Iron low-ionization (FeLoBAL) BAL QSOs show additional absorption from excited states of Fe II and Fe III (e.g. Hall et al. 2002). About 15 per cent (Knigge et al. 2008) of the whole population of quasars are classified as BAL, although some authors (Ganguly et al. 2007) suggest that the intrinsic fraction could be much higher.

Powerful outflows can enrich the quasar host galaxy interstellar medium, contributing to a variety of feedback effects such as regulating host galaxy star formation rates (Hopkins & Elvis 2010),

★ E-mail: diego.tuccillo@obspm.fr (DT); bruni@mpifr-bonn.mpg.de (GB)

© 2017 The Authors
Published by Oxford University Press on behalf of the Royal Astronomical Society

Downloaded from https://academic.oup.com/mnras/article-abstract/467/4/4763/2978044 by Universidad de Cantabria user on 09 July 2019

and limiting quasar lifetimes by removing fuel from the nuclear regions (Silk & Rees 1998). Understanding the physics behind BAL outflows may be fundamental to disclose the connection between the evolution of quasars and their host galaxies. According to the *orientation scenario*, BAL QSOs are normal quasars seen at high inclination angles, and the outflows at the origin of the BAL features are located near the equatorial plane of the accretion disc. This model fits naturally in the active galactic nucleus (AGN) unification models (Antonucci 1993; Urry & Padovani 1995) and it is supported by the claim that both BAL and non-BAL QSOs appear to be drawn by the same parent population (Reichard et al. 2003). However, the orientation scenario is contradicted from the studies on the radio-loud (RL) BAL QSOs, studied for the first time in Brotherton et al. (1998) and in Becker et al. (2000). In fact, an edge-on geometry should lead to lobe-dominated emission and thus a steep radio spectrum but, using large samples of RL BAL QSOs (Montenegro-Montes et al. 2008; DiPompeo et al. 2011; Fine, Jarvis & Mauch 2011; Bruni et al. 2012), it has been confidently established that these objects have a variety of spectral indices for their radio spectral energy distribution (SED hereafter). Recently, other authors have confirmed this by mean of an emission lines study for a sample of BAL and non-BAL quasars (Matthews et al 2017). In light of these results, a pure orientation scenario is clearly inadequate to explain the full extent of the BAL phenomena, especially considering that most of the continuum and emission-line properties of RL and radio-quiet (RQ) BALs appear statistically identical and therefore suggest that the results obtained on RL QSOs can be extended to their RQ counterparts (Bruni et al. 2014; Rochais et al. 2014). The other main model proposed to explain the nature of BAL QSOs is an *evolutionary model* as discussed for example by Lípari & Terlevich (2006). According to this, BAL QSOs represent a particular evolutionary stage of quasars, during which absorbing material with a high covering fraction is being expelled from the central regions of the quasar. The RL systems may be associated with the later stages of evolution (Becker et al. 1997), when jets have removed the clouds responsible for the generation of BALs. The early claim that BAL QSOs have redder continua has been confirmed by a number of different studies in the UV/optical domain (Weymann et al. 1991; Sprayberry & Foltz 1992; Brotherton et al. 2001; Reichard et al. 2003; Urrutia et al. 2009) and it has been pointed out in support of the evolutionary scenario because it is in agreement with the dustier environment expected in a young AGN. However, the results of the studies at higher wavelengths are controversial (Gallagher et al. 2007; DiPompeo et al. 2013). It has also been proved that RL BAL QSOs show a variety of possible radio morphologies (Montenegro-Montes et al. 2008; DiPompeo et al. 2011; Bruni et al. 2012; Bruni et al. 2013) and are not always unresolved, as it may be expected for young radio sources (Fanti et al. 1990).

One of the most successful and studied BAL catalogues is the one from Gibson et al. (2009) that includes 5039 BAL QSOs, and the most recent Quasar Catalog (Paris et al. 2017) based on the Sloan Digital Sky Survey Data Release 12 (SDSS DR12) includes ∼30 000 BAL QSOs. In spite of these large samples of BAL QSOs and the proved interest of the radio studies on this population, there is still a lack of observational information about RL BAL QSOs at high redshifts. In fact, these studies are hampered by the lower radio flux density collected at higher redshift and strongly bounded by the scarce number of RL BAL QSOs known at $z > 3$. RL QSOs account only for 8–13 per cent of QSOs (Ivezić et al. 2002; Jiang et al. 2007; Baloković et al. 2012), and the density of quasars is a strong function of redshift that peaks at $z \sim 2$–3 and declines exponentially towards lower and higher redshift (e.g. Boyle et al. 2000). Finally, the identification of BAL QSOs is limited in SDSS at $z \lesssim 4.9$, since absorption in high-ionization species like C IV 1550 Å is required for the classification of a quasar as a BAL. As a result, the limit in redshift for the work of Montenegro-Montes et al. (2008) was $z = 3.4$ while the samples of DiPompeo et al. (2011) and Bruni et al. (2012) had a maximum of $z = 3.42$ and 3.38, respectively. Extension of the samples to higher redshift is an important test to look for evolutionary trends in BAL properties. Indeed, Allen et al. (2011) already found a dependence on redshift of the BAL QSO fraction, the latter decreasing by a factor 3.5 ± 0.4 from redshifts $z \sim 4.0$ down to ~ 2.0, and they interpret this as an evolutionary behaviour, not reproducible by the orientation model alone.

In this work, we aim to complete the radio property studies carried out by previous authors, filling the gap of information $3.6 \leq z \leq 4.8$. For this purpose, we selected and collected the radio flux densities of a sample of 15 RL BAL QSOs and 14 normal RL QSOs matched in redshift and magnitude. We observed these QSOs at six different frequencies in order to reconstruct their SED. The age and orientation of the radio jet are estimated from the SED. In particular, the spectral index is used as a statistical indicator of the orientation of the jet with respect to the observer's line of sight, thus helping in verifying a possible preferred orientation. The number of gigahertz peaked spectrum (GPS) sources is used as indicative of whether these objects are typically younger than a sample of 'normal' QSOs. Imaging synthesis, possible with the interferometric observations, is used to give indications about the extension and morphology of these sources.

We also used a larger sample of 22 RL high-redshift BAL QSOs to compare their broad-band optical colours with those of 113 RL QSOs with $3.6 \leq z \leq 4.8$. This way, we investigate the question of the continuum differences between BAL QSOs and non-BAL QSOs, comparing our results with those from other authors (Menou et al. 2001; Tolea, Krolik & Tsvetanov 2002; Reichard et al. 2003) at lower redshift or for samples of RQ BALs.

In the same range of redshift $3.6 \leq z \leq 4.8$, we also used a larger sample of 22 RL high-redshift BAL QSOs to compare their broad-band optical colours with those of 113 normal RL QSOs with comparable redshift. This way, we investigate the question of the continuum differences between BAL QSOs and non-BAL QSOs, comparing our results with those from other authors (Menou et al. 2001; Tolea et al. 2002; Reichard et al. 2003) at lower redshift or for samples of RQ BALs.

In this paper, we adopt the Λ cold dark matter cosmology with $\Omega_\Lambda = 0.7$, $\Omega_\mathrm{m} = 0.3$ and $H_0 = 70\,\mathrm{km\,s^{-1}\,Mpc^{-1}}$.

2 THE HIGH-REDSHIFT RL BAL QSO SAMPLE

We selected a sample of spectroscopically identified RL BAL QSOs with $3.6 \leq z \leq 4.8$ and detected in both SDSS DR7 and FIRST. The range of redshifts was chosen in order to mostly overlap the one used in Tuccillo, González-Serrano & Benn (2015), where we used a neural network machine method to select RL QSO candidates in the redshift range $3.6 \leq z \leq 4.4$. This selection method was proven to be highly complete (97 per cent) and it allowed the spectroscopic identification of 15 QSOs missed in SDSS DR7 (Carballo et al. 2008; Tuccillo et al. 2015). The reduced biases in the selection lead to a very accurate estimation of the optical luminosity function (LF) of RL QSOs in this range of redshift. Exploring a similar range of redshift, we search for BAL QSOs within a very complete spectroscopic sample of RL QSOs. Moreover, the careful determination of the quasar LF assures that the RQ and the RL QSO populations do not evolve differently in this range of redshift. Therefore, any

Downloaded from https://academic.oup.com/mnras/article-abstract/467/4/4763/2978044 by Universidad de Cantabria user on 09 July 2019

Table 1. Sample of 22 RL BAL selected from sources matched in FIRST and SDSS DR7.

SDSS ID	ID	RA	Dec.	i_{AB}	$S_{1.4\,GHz}$	z	$\log_{10} P_{1.4\,GHz}$	$\log_{10} R$	AI*	Note
		(J2000)			(mJy)		(W Hz^{-1})	(mag)	(km s^{-1})	
(1)	(2)	(3)		(4)	(5)	(6)	(7)	(8)	(9)	(10)
J000051.57+001202.5	0000+00	00:00:51.57	+00:12:02.5	19.95	2.99	4.00	26.15	2.16	3762.29	(a), (g), (p)
J074738.49+133747.3	0747+13	07:47:38.49	+13:37:47.3	19.15	6.62	4.04	26.53	2.13	5879.09	
J094003.03+511602.7	–	09:40:03.03	+51:16:02.7	18.77	13.91	3.60	26.76	2.33	166.42	
J100645.59+462717.2	1006+46	10:06:45.59	+46:27:17.2	19.81	6.32	4.44	26.58	2.65	185.31	
J102343.13+553132.4	1023+55	10:23:43.13	+55:31:32.4	19.31	2.80	4.45	26.23	2.25	4820.07	(a), (g)
J103601.03+500831.8	1036+50	10:36:01.03	+50:08:31.8	19.20	9.22	4.47	26.75	2.65	1737.88	(a), (g)
J110946.44+190257.6	1109+19	11:09:46.44	+19:02:57.6	20.03	6.95	3.67	26.47	2.46	1678.28	(p)
J111055.22+430510.1	1110+43	11:10:55.22	+43:05:10.1	18.21	1.21	3.82	25.75	1.11	193.72	(p)
J112938.73+131232.3	1129+13	11:29:38.73	+13:12:32.3	18.76	1.33	3.61	25.74	1.22	206.46	(p)
J113330.91+380638.2	–	11:33:30.91	+38:06:38.2	19.66	0.87	3.63	25.56	1.42	176.29	(g), (p)
J115731.67+225726.4	1157+22	11:57:31.67	+22:57:26.4	20.14	3.81	3.92	26.26	2.32	979.66	(p)
J120447.15+330938.7	–	12:04:47.15	+33:09:38.7	18.38	0.92	3.61	25.58	1.25	6534.97	(a), (g), (p)
J124658.83+120854.7	–	12:46:58.83	+12:08:54.72	19.86	1.44	3.80	25.82	1.76	1519.70	(a), (g), (p)
J130348.94+002010.5	–	13:03:48.94	+00:20:10.51	18.66	0.99	3.65	25.62	1.15	1032.38	(a), (g), (p)
J133234.18+000921.7	1332+00	13:32:34.18	+00:09:21.7	20.30	1.49	3.66	25.80	1.95	149.60	(t)
J134428.55+625608.2	1344+62	13:44:28.55	+62:56:08.2	19.23	2.58	3.67	26.04	1.77	4967.82	(t), (g)
J134854.37+171149.6	1348+17	13:48:54.37	+17:11:49.6	18.91	1.89	3.62	25.90	1.52	356.61	(p)
J135554.56+450421.0	–	13:55:54.56	+45:04:21.0	19.31	2.07	4.09	26.03	1.62	330.64	(g)
J150643.81+533134.5	1506+53	15:06:43.81	+53:31:34.5	18.77	14.63	3.79	26.82	2.34	166.89	(t)
J151146.99+252424.3	1511+25	15:11:46.99	+25:24:24.3	19.76	1.39	3.72	25.78	1.72	3034.72	(a), (p)
J161716.49+250208.1	–	16:17:16.49	+25:02:08.1	19.83	2.35	3.94	26.06	1.95	4439.58	(a), (g), (p)
J165913.23+210115.8	1659+21	16:59:13.23	+21:01:15.8	20.11	28.81	4.78	27.30	3.37	787.91	

The columns give the following: (1) SDSS object-ID; (2) shortened name assigned to source for the radio observations, sources without this ID were not used for our radio studies; (3) SDSS J2000 coordinates; (4) SDSS i-magnitude corrected for galactic extinction; (5) FIRST integrated radio flux density; (6) QSO redshift; (7) radio luminosity at 1.4 GHz; (8) R-parameter of radio-loudness (Kellermann et al. 1989); (9) modified absorption index AI* (Bruni et al. 2012); (10) note indicating if the QSO is classified as BAL in previous catalogues, (a) Allen et al. (2011), (g) Gibson et al. (2009) (t) Trump et al. (2006) (p) Pâris et al. (2012).

possible difference found in this research between BAL and non-BAL QSOs is not a priori biased by different evolutions between RL and RQ populations.

A simple one-to-one match between FIRST and SDSS will miss double-lobe QSOs without detected radio cores. de Vries, Becker & White (2006) found that for a sample of 5515 FIRST-SDSS QSOs with radio morphological information within 450 arcsec, the fraction of FIRST-SDSS double-lobe QSOs with undetected cores is 3.7 per cent. Since the starting samples of SDSS QSOs in de Vries et al. (2006) and in this work obey similar SDSS selection criteria, we estimate that our sample is similarly affected for this source of incompleteness.

All the sources of our sample are RL in agreement with both the main definitions adopted in the literature to consider a quasar as 'RL'. In particular, they meet the criteria based on the total radio luminosity of the source adopted by Gregg et al. (1996), i.e. $\log P_{1.4,GHz}(\mathrm{W\,Hz^{-1}}) > 25.5$. They also have $R > 10$, a commonly used threshold to define radio-loudness on the basis of the R-parameter, defined as the rest-frame ratio of the monochromatic 6-cm (5 GHz) and 2500 Å flux densities (Kellermann et al. 1989; Stocke et al. 1992). We also note that, given the high redshift of our sample of BAL QSO, we cannot measure the transition lines needed to distinguish our BAL QSOs sample in Hi-, Lo- or FeLoBAL QSOs, and therefore our sample is likely to include more than just one subclass of BALs.

In Section 2.1, we give the details of our selection of BAL QSOs.

2.1 BAL QSOs selection criteria

We started our selection considering the sample of 222 517 sources obtained cross matching each source of the FIRST survey (2003 April 11 version), not flagged as a possible sidelobe or nearby bright source (∼3.6 per cent of the sources in the FIRST catalogue), with the closest optical object in the 'PhotoPrimary' view of the SDSS DR7 catalogue within a 1.5 arcsec radius. In this sample, there is no selection by radio flux density or radio morphology other than the requirement that the radio source have at least a weak core component. From this sample, we discarded all the sources not classified as 'point-like' or tagged with the 'fatal' error flags by the SDSS pipelines. In this way, we pre-selected a sample of 36 267 sources.

At this point, we searched for all the available optical spectra for the sources of this sample, either from the SpecObj view of SDSS-DR7 or from the 5th edition of the SDSS Quasar Catalogue (DR7 QSO Catalogue; Schneider et al. 2010). We integrated the sample with all the new quasars discovered with our neural network selection strategies (Tuccillo et al. 2015). We visually inspected all the spectra of the sources classified as QSOs at $z > 3$ in the DR7 QSO catalogue or in SDSS-DR7, looking for a broad absorption trough in the Ci IV line.

Finally, we measured the absorption in the Ci IV for a rigorous and homogeneous selection of the final sample of BAL QSOs. In the literature, there is more than one metric used to separate BAL QSOs and non-BAL QSOs on the basis of the measured absorption. The most widely used definitions are (i) the *balnicity index* (BI, first presented by Weymann et al. 1991); (ii) the *absorption index* (AI; Hall et al. 2002; Trump et al. 2006), designed to include narrower troughs than the BI; and (iii) the *modified balnicity index* BI_0 (Gibson et al. 2009), which extends the integration region to zero velocity. In this work, to discriminate between BAL and not-BAL QSOs, we choose to apply the same criteria used in Bruni et al. (2012), in order to compare our results with their studies at lower

Downloaded from https://academic.oup.com/mnras/article-abstract/467/4/4763/2978044 by Universidad de Cantabria user on 09 July 2019

redshift. Therefore, we calculated the AI, as defined by Hall et al. (2002):

$$AI = \int_{0\,\mathrm{km\,s^{-1}}}^{25\,000\,\mathrm{km\,s^{-1}}} \left(1 - \frac{f(v)}{0.9}\right) C\,\mathrm{d}v, \quad (1)$$

where $f(v)$ is the continuum-normalized flux (unsmoothed whenever possible) as a function of velocity v, relative to the line centre. We integrate the spectral region between the peaks of the C IV and Si IV emission lines to up to 25 000 km s^{-1} from the former. The constant C is posed to be equal to 1 when $f(v)$ is less than 0.9 for at least 1000 km s^{-1} (as in Trump et al. 2006), and it is posed to be equal to 0 elsewhere. We considered as genuine BAL QSOs only objects with an $AI > 100$ km s^{-1}. Applying this criteria, we ended-up with a sample of 22 BAL QSOs within $3.6 \leq z \leq 4.8$. Comparing (see Table 1) this sample with larger catalogues of BALs that are also based on the SDSS and therefore overlapping the sky area of our sample, we verified that nine of the sources included in our sample are included also in the catalogue of Allen et al. (2011), 10 are included also in the Gibson catalogue (Gibson et al. 2009) and three are included also in the catalogue from Trump et al. (2006). Twelve QSOs are also classified as BAL in the DR12 QSO Catalog (Pâris et al. 2012), published after our selection. Nine BALs of our sample were not classified as such in the literature at the moment of the selection, and four have been identified as BAL QSOs in this work for the first time.

Table 1 provides a catalogue of the 22 BAL QSOs of our sample. In the table, we include the measure of the AI for each BAL QSO and we indicate which of these sources were used for the radio studies that we will discuss in the next section. As a whole, and as shown in Fig. 1, our sample of 22 RL BAL QSOs extends the samples used in DiPompeo et al. (2011) and Bruni et al. (2012), for the redshift range covered (out to $z = 4.8$), to lower optical and radio flux densities.

3 RADIO OBSERVATIONS AND DATA REDUCTION

With the aim of repeating at high redshift radio studies similar to those of Montenegro-Montes et al. (2008), DiPompeo et al. (2011) and Bruni et al. (2012), we originally proposed to observe the 22 BAL QSOs of our sample and a 'comparison sample' of 22 unabsorbed QSOs in multiple frequency bands, including 1.4 (L band), 4.9 (C band), 8.4 (X band) and 22 GHz (K band) at the 100-m Effelsberg Telescope and at the EVLA radio-array in the A configuration. Not all sources of the samples were observed, either because they were too faint in radio or because of technical problems related to bad weather. None the less, the final observed sample, composed of 15 (out of the 22) BAL QSOs, and 14 QSOs of the 'comparison sample', provided sufficient statistic to complete the planned studies.

In Table 1 of Section 2.1, we have indicated the 15 BAL QSOs for which the data provide significant frequency coverage to analyse the full shapes of the radio spectrum. In Section 3.1, we give the details of the criteria used to build the 'comparison sample' of normal RL QSOs, and we will present the catalogue of the 14 used for the radio studies discussed in this section.

3.1 Comparison sample

The 'comparison sample' was extracted from the spectroscopically identified non-BAL RL QSOs included in the sample of 36 267 preselected sources presented in Section 2.1. The sample was selected

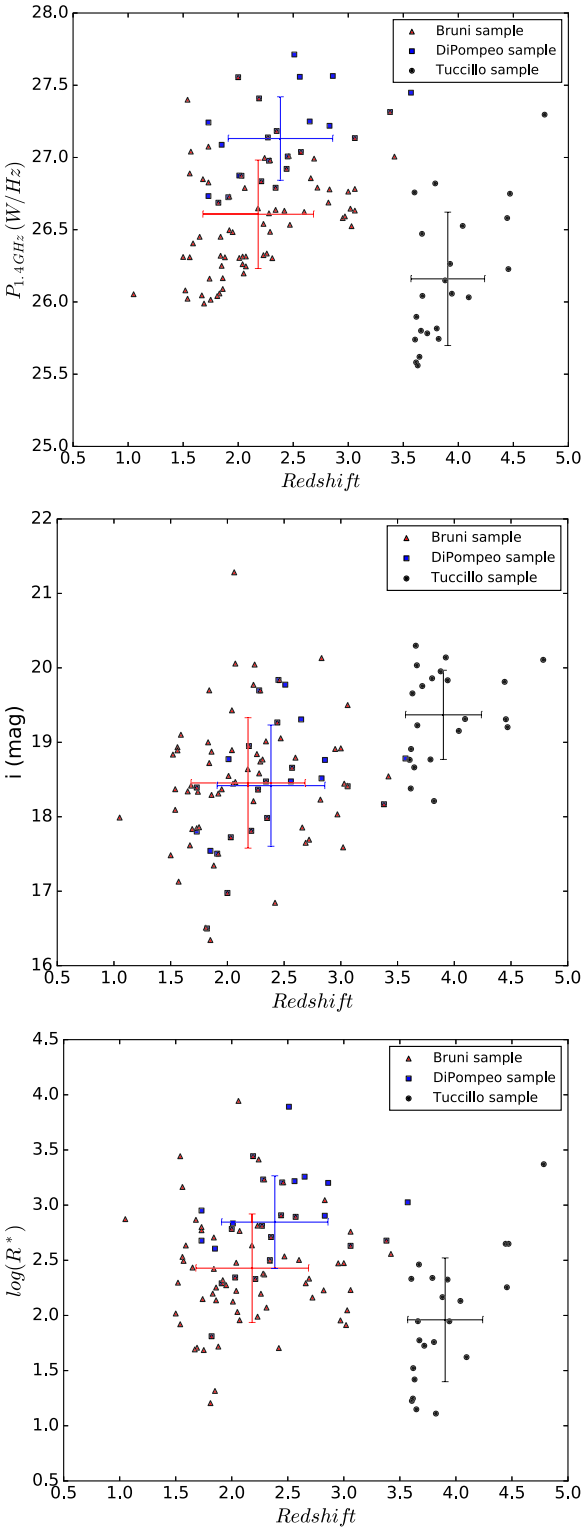

Figure 1. We show, as a function of the redshift, the distributions in radio luminosity [at $\log_{10} P_{1.4\mathrm{GHz}}$ (W Hz^{-1})], i-magnitude and radio-loudness R for the 25 RL BAL QSOs (red triangles) used in Bruni et al. (2012), for the 74 RL BAL QSOs (blue squares) used in DiPompeo et al. (2011) and for the 22 RL BAL QSOs (black dots) used in this work. The large crosses with the 1σ error bar represent the location of the mean for each of the plotted samples. The sample studied in this work was selected in order to extend the previous cited studies at higher redshift and at lower optical and radio fluxes, probing new parameter space. See Section 2.1.

Downloaded from https://academic.oup.com/mnras/article-abstract/467/4/4763/2978044 by Universidad de Cantabria user on 09 July 2019

Table 2. Comparison sample of non-BAL QSOs observed with the Effelsberg-100 m single dish and/or the JVLA interferometer.

SDSS ID	ID	RA (J2000)	Dec.	i_{AB}	$S_{1.4GHz}$ (mJy)	z	$\log_{10} P_{1.4GHz}$ (W Hz^{-1})	$\log_{10} R$ (mag)
(1)	(2)	(3)		(4)	(5)	(6)	(7)	(8)
J030025.23+003224.2	0300+00	03:00:25.23	+00:32:24.2	19.68	7.69	4.18	26.62	2.31
J083322.50+095941.2	0833+09	08:33:22.50	+09:59:41.2	18.60	125.76	3.73	27.74	3.18
J084044.19+341101.6	0840+34	08:40:44.19	+34:11:01.6	19.58	13.59	3.89	26.81	2.64
J090129.23+104240.4	0912+10	09:01:29.23	+10:42:40.4	20.08	2.14	3.96	26.02	2.01
J091824.38+063653.4	0918+06	09:18:24.38	+06:36:53.4	19.18	26.50	4.19	27.16	2.88
J101747.76+342737.9	1017+34	10:17:47.76	+34:27:37.9	19.99	2.64	3.69	26.06	2.02
J110201.91+533912.6	1102+53	11:02:01.91	+53:39:12.6	20.31	5.57	4.30	26.50	2.51
J112530.50+575722.7	1125+57	11:25:30.50	+57:57:22.7	19.44	2.99	3.68	26.11	1.85
J115045.61+424001.1	1150+42	11:50:45.61	+42:40:01.1	19.87	1.51	3.87	25.85	1.72
J124943.67+152707.1	1249+15	12:49:43.67	+15:27:07.1	19.05	2.00	3.99	26.00	1.61
J131121.32+222738.7	1311+22	13:11:21.32	+22:27:38.7	20.19	6.53	4.61	26.62	2.84
J142326.48+391226.3	1423+39	14:23:26.48	+39:12:26.3	20.04	6.51	3.92	26.50	2.46
J144643.37+602714.4	1446+60	14:46:43.37	+60:27:14.4	19.74	1.80	3.78	25.91	1.77
J161105.65+084435.4	1611+08	16:11:05.65	+08:44:35.4	18.84	8.82	4.54	26.74	2.31

The columns give the following: (1) SDSS object-ID; (2) shortened name assigned to source for the radio observations; (3) SDSS J2000 coordinates; (4) SDSS *i*-magnitude corrected for galactic extinction; (5) FIRST integrated radio flux density; (6) QSO redshift; (7) radio luminosity at 1.4 GHz; (8) *R*-parameter of radio-loudness (Kellermann et al. 1989).

using the same criteria applied in DiPompeo, Brotherton & De Breuck (2012), i.e. searching for each BAL QSOs of our sample, a correspondent non-BAL RL QSO matched within 20 per cent of SDSS *i*-band magnitude, 20 per cent of 1.4 GHz radio flux density and 10 per cent of redshift.

Table 2 provides a catalogue of the 14 non-BAL QSOs of the comparison samples for which the radio data provide significant frequency coverage to analyse the full shape of the radio spectrum. Fig. 2 shows that these 14 non-BAL QSOs and the 15 observed BAL QSOs are still well matched in redshift, optical magnitude and radio flux density.

As a whole, the sample of 29 RL QSOs (15 BAL and 14 non-BAL) that we observed extends the samples used in DiPompeo et al. (2011) and Bruni et al. (2012), for the redshift range covered (out to $z = 4.8$), and extend to lower optical and radio fluxes. In particular, for their list of 25 radio-bright ($S_{1.4\,GHz} > 30$ mJy) RL QSOs with $1.73 \leq z \leq 3.38$, Bruni et al. (2012) collected radio flux densities from 1.4 to 43 GHz, including observations with the Effelsberg telescope at the same frequencies (2.6, 4.8 and 8.3 GHz) that we use and observations at 1.4, 4.86 and 8.46 GHz with the Very Large Array (VLA) in C configuration. For their sample of 74 ($S_{1.4\,GHz} > 10$ mJy) RL BAL QSOs with $1.5 \leq z \leq 3.42$, DiPompeo et al. (2011) collected flux densities at 4.9 and 8.4 GHz with the VLA (in D- and DnC-array configuration) telescope, and completed their observations with the FIRST integrated 1.4 GHz flux densities. Our radio observations including the same, or close, frequencies used in the two cited works significantly increase their sample size and therefore determine whether the spectral index distribution differences identified remain robust. This allows us to test not only the orientation properties for a higher redshift population, but also a larger range of radio brightness.

3.2 Observational campaign

The observational campaign carried out for this work included both interferometric (Jansky Very Large Array – JVLA) and single-dish (Effelsberg-100 m) observations. In the following, details about observing set-up and strategy, as well as data reduction process, are given. See Table 3 for a summary of observations set-ups, including observing frequencies and beam sizes for both telescopes.

JVLA

During 2012 November, we performed observations at the JVLA at 1.5, 5.5 and 9 GHz, with the aim of adding high-sensitivity flux density measurements, and obtain morphological information. All observations were performed in the A configuration, and in dynamic mode, with 1 or 1.5 h slots. Phase referencing was applied to all sources, and standard flux density calibrators were observed at least once for every slot. A minimum rms of ∼0.1 mJy was obtained. Data were reduced with the latest stable version of the CASA[1] software (4.1.0), making use of customized reduction scripts run on the MPIfR High-Performance Computer cluster (HPC). Flux densities were extracted via bi-dimensional Gaussian fit on the produced maps. Errors were calculated assuming a 5 per cent uncertainty for the absolute flux density calibration and quadratically adding it to the map rms. Given the wide bandwidth available, we split it in two equal intervals, taking as a reference the central frequency, to improve the frequency coverage.

Effelsberg-100 m telescope

Observations with the Effelsberg-100 m single dish were performed in different runs, initially as a granted-time project in 2012 September, and later continued as a filler project, to improve frequency coverage, until 2015 May. The cross-scan observing mode was used, at three different frequencies (2.6, 4.8 and 8.3 GHz), increasing the number of subscan repetitions depending on the source faintness and reaching a maximum of 20 min observing time per frequency, at which a minimum rms of ∼1 mJy can be reached. Pointing on sources near to target was performed every time the telescope significantly changed the elevation to compensate for gravitational deformations of the antenna. Data were reduced with the latest version of the TOOLBOX[2] software reduction package. The flux density

[1] http://casa.nrao.edu/index.shtml
[2] https://eff100mwiki.mpifr-bonn.mpg.de/doku.php

Downloaded from https://academic.oup.com/mnras/article-abstract/467/4/4763/2978044 by Universidad de Cantabria user on 09 July 2019

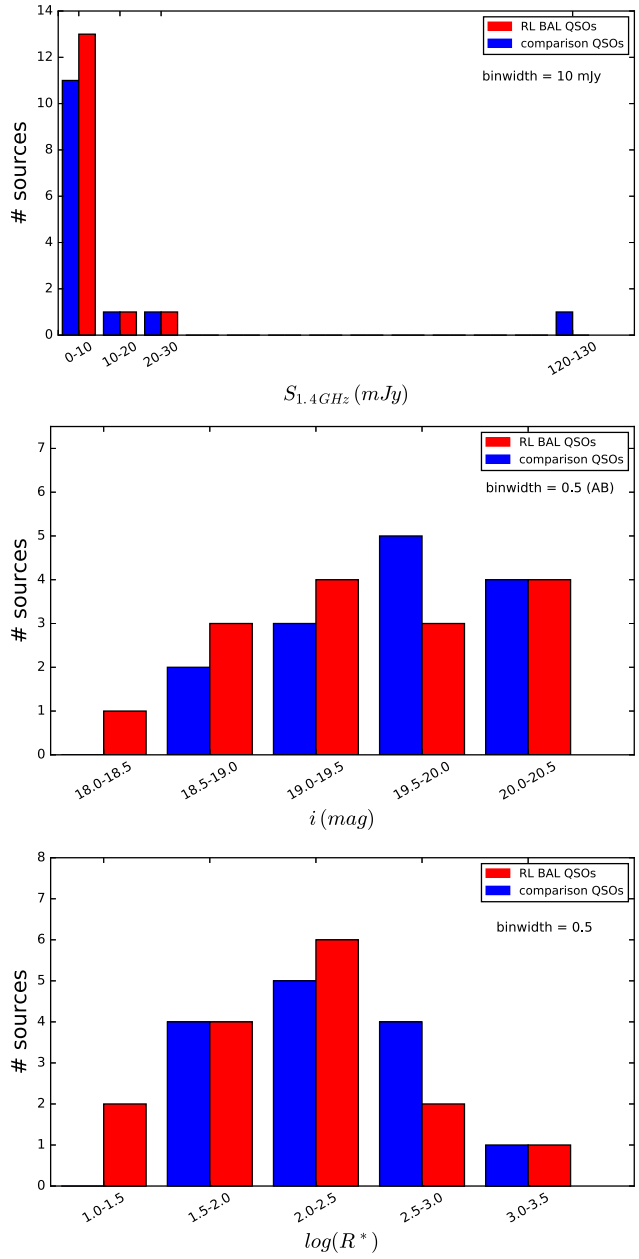

Figure 2. We present the distributions in radio power (FIRST integrated radio flux density), *i*-magnitude and radio-loudness *R* of 15 RL BAL QSOs (red bins) and 14 normal RL QSOs (blue bins) having $3.6 \leq z \leq 4.8$, as listed in Tables 1 and 2. For all these sources, we had significant frequency coverage to analyse the full shapes of the radio spectrum. The two samples are well matched in optical magnitude and radio flux density. See Section 3.1.

Table 3. Observing frequencies and beam sizes (half-power beamwidth).

Telescope	Frequency (GHz)	Bandwidth (MHz)	$\theta_{\rm HPBW}$ (arcsec)
Effelsberg-100 m	2.64	80	265
Effelsberg-100 m	4.85	500	145
Effelsberg-100 m	8.35	1100	80
JVLA(A)	1.5	1024	1.3
JVLA(A)	5.5	2048	0.33
JVLA(A)	9.0	2048	0.20

scale was calibrated on well-known sources observed every ∼4 h (3C286, 3C48, 3C295) using the flux densities from Baars et al. (1977). Flux densities were extracted via Gaussian fit of the cross-scans. Errors were calculated assuming a 10 per cent uncertainty for the absolute flux density calibration (given the variable weather conditions during the campaign) and adding it via quadratic sum to the cross-scan rms. 3σ upper limits are given for non-detections.

4 OBSERVATIONAL RESULTS

The collected flux densities are reported in Tables 4 and 5. In total, 20 sources were observed with the JVLA, and 26 with the Effelsberg-100 m. When no detections at 1.5 GHz were available from our campaign, we used the measurement at 1.4 GHz from the FIRST survey.

Despite observations at the Effelsberg-100 m telescope having been carried out on a 3-yr time window, the obtained SED does not show significant changes along frequencies that might suggest a strong variability. Thus, we can safely combine data from this campaign to obtain the desired frequency coverage.

4.1 Morphology

All the observed sources are unresolved both with the Effelsberg-100 m and with the JVLA in the A configuration. Considering the angular resolution of the latter for the eight BAL and eight non-BAL QSOs detected at 9 GHz (0.2 arcsec), we obtain an upper limit for the projected linear size of 1.4 kpc at the mean redshift of 4.02 and 3.91 for our BAL and non-BAL samples. This is compatible with the typical linear size of high frequency peakers (HFP, 0.01–0.5 kpc; Dallacasa et al. 2000) and also GPS sources (0.5–5 kpc; O'Dea 1998). Further Very Long Baselines Interferometry (VLBI) observations would be required to resolve sources at these redshifts.

4.2 SED shape and spectral index

In the following, we analyse the SEDs in order to get information about the orientation and age of our high-redshift sample.

Synchrotron peak frequencies

The collected flux densities between 1.25 and 9.5 GHz allow us to reconstruct the SED of our objects in a reasonable way. When no measurements from our campaign were available at 1.5 GHz, we used data from the FIRST survey. In Figs 3 and 4, the SEDs for each source are presented. We can get an indication of the presence of a peak in order to obtain the fraction of young radio sources in our samples. Indeed, GPS sources at lower redshifts are usually identified as objects peaking in the range 1 GHz $\leq \nu_{\rm peak} \leq$ 8 GHz (O'Dea 1998) while HFP can peak at frequencies >8 GHz (Dallacasa et al. 2000). Both are generally interpreted as young radio sources, in an evolutionary track towards compact steep spectrum sources, peaking at hundreds of MHz (Saikia & Salter 1988; Fanti et al. 1990) as the emitting plasma adiabatically expands. Considering the redshift range of our sample (mean redshift ∼4), the peaking interval of GPS and HFP translates – in the observer's frame – into an interval between 0.2 and 1.6 GHz for the first (outside our observing window) and >1.6 GHz for the latter.

We performed SED fitting using two simple functions: a power law ('L' hereafter) describing the optically thin part of the synchrotron emission and a parabola in logarithmic scale ('P' hereafter) as a simplified version of the peaked synchrotron emission, including the optically thin/thick parts. The aim was to determine, via chi-squared minimization, which among our sources present a peak

Downloaded from https://academic.oup.com/mnras/article-abstract/467/4/4763/2978044 by Universidad de Cantabria user on 09 July 2019

Table 4. Flux densities (mJy) collected in the radio band for the 15 high-redshift BAL QSOs. Measurements at 1.25, 1.75, 5, 6, 8.5 and 9.5 GHz are from the JVLA, while those at 2.6, 4.8 and 8.3 GHz are from the Effelsberg-100 m single dish. Asterisked values at 1.4 GHz come from the FIRST survey. In the last three columns, the spectral index, fit type and peak frequency in the observer's frame (in GHz) are given.

Source	$S_{1.25}$	$S_{1.4}$	$S_{1.75}$	$S_{2.6}$	$S_{4.8}$	S_5	S_6	$S_{8.3}$	$S_{8.5}$	$S_{9.5}$	α	Fit	Peak
0000+00	2.0 ± 0.1	–	1.4 ± 0.2	<11	–	0.8 ± 0.1	0.7 ± 0.1	–	0.8 ± 0.1	0.7 ± 0.1	−0.00 ± 0.29	L	–
0747+13	–	8.0 ± 0.8*	–	12 ± 4	13 ± 2	–	–	6 ± 1	–	–	−1.41 ± 0.37	P	3.14
1006+46	–	6.3 ± 0.6*	–	12 ± 1	8 ± 1	–	–	5 ± 1	–	–	−0.86 ± 0.38	P	3.02
1023+55	4.1 ± 0.3	–	4.8 ± 0.4	<23	4 ± 1	2.1 ± 0.1	1.4 ± 0.1	–	1.6 ± 0.1	1.5 ± 0.1	−0.51 ± 0.13	P	1.99
1036+50	–	9.2 ± 1.0*	–	7 ± 1	5 ± 1	–	–	3 ± 1	–	–	−0.93 ± 0.63	P	0.56
1109+19	7.2 ± 0.5	–	5.7 ± 0.3	6 ± 1	–	2.8 ± 0.1	2.4 ± 0.1	–	1.7 ± 0.1	1.5 ± 0.1	−0.94 ± 0.11	P	0.29
1110+43	–	1.2 ± 0.2*	–	–	3 ± 1	–	–	3 ± 1	–	–	0.00 ± 0.77	P	6.31
1129+13	7.0 ± 1.5	–	2.1 ± 0.2	–	–	1.0 ± 0.1	0.6 ± 0.1	–	0.5 ± 0.1	0.4 ± 0.1	−1.31 ± 0.36	P	0.97
1157+22	2.4 ± 0.1	–	2.1 ± 0.1	–	–	2.2 ± 0.1	1.9 ± 0.1	–	1.3 ± 0.1	1.1 ± 0.1	−0.99 ± 0.15	P	3.05
1332+00	2.7 ± 0.2	–	1.8 ± 0.1	–	–	0.7 ± 0.1	0.7 ± 0.1	–	0.5 ± 0.1	0.5 ± 0.1	−0.63 ± 0.40	L	–
1344+62	2.0 ± 0.3	–	2.3 ± 0.2	<6	–	0.9 ± 0.1	0.7 ± 0.1	–	–	–	−1.38 ± 0.30	P	1.77
1348+17	2.0 ± 0.3	–	1.7 ± 0.1	4 ± 1	–	3.1 ± 0.2	3.0 ± 0.2	–	2.6 ± 0.1	2.5 ± 0.2	−0.33 ± 0.12	P	4.85
1506+53	–	14.6 ± 1.5*	–	14 ± 3	–	–	–	7 ± 2	–	–	−0.60 ± 0.58	P	1.70
1511+25	–	1.2 ± 0.2*	–	–	<12	–	–	8 ± 2	–	–	1.07 ± 0.49	L	–
1659+21	29.1 ± 1.5	–	24.6 ± 1.3	20 ± 2	16 ± 4	12.1 ± 0.6	10.2 ± 0.5	–	7.9 ± 0.5	6.9 ± 0.4	−0.80 ± 0.13	P	0.16

Table 5. Flux densities (mJy) in the radio band collected for the 14 high-redshift non-BAL QSOs. Measurements at 1.25, 1.75, 5, 6, 8.5 and 9.5 GHz are from the JVLA, while at 2.6, 4.8 and 8.3 GHz are from the Effelsberg-100 m single dish. Asterisked values at 1.4 GHz comes from the FIRST survey. In the last three columns, the spectral index, fit type and peak frequency in the observer's frame (in GHz) are given.

Source	$S_{1.25}$	$S_{1.4}$	$S_{1.75}$	$S_{2.6}$	$S_{4.8}$	S_5	S_6	$S_{8.3}$	$S_{8.5}$	$S_{9.5}$	α	Fit	Peak
0300+00	6.4 ± 0.4	–	7.5 ± 0.4	6 ± 1	–	4.3 ± 0.2	3.5 ± 0.2	–	1.4 ± 0.1	1.3 ± 0.1	−2.11 ± 0.14	P	2.13
0833+09	–	126 ± 12*	–	106 ± 11	88 ± 9	–	–	77 ± 14	–	–	−0.24 ± 0.34	L	–
0840+34	–	13.6 ± 0.1*	–	15 ± 2	31 ± 6	–	–	8 ± 1	–	–	−2.47 ± 0.38	P	4.26
0901+10	3.4 ± 0.5	–	2.0 ± 0.3	–	–	0.8 ± 0.1	0.6 ± 0.1	–	0.4 ± 0.1	0.3 ± 0.1	−1.31 ± 0.46	L	–
0918+06	–	26.5 ± 2.6*	–	43 ± 4	36 ± 4	–	–	23 ± 4	–	–	−0.82 ± 0.34	P	3.15
1017+34	–	2.6 ± 0.3*	–	7 ± 1	11 ± 1	–	–	–	–	–	0.74 ± 0.28	P	5.98
1102+53	–	5.6 ± 0.6*	–	6 ± 1	6 ± 1	–	–	6 ± 1	–	–	−0.00 ± 0.38	L	–
1125+57	2.3 ± 0.2	–	2.0 ± 0.1	–	–	0.8 ± 0.1	0.6 ± 0.1	–	0.5 ± 0.1	0.5 ± 0.1	−0.89 ± 0.38	P	0.84
1150+42	3.0 ± 0.2	–	2.0 ± 0.2	–	–	0.5 ± 0.1	0.4 ± 0.1	–	<0.3	<0.3	−1.73 ± 0.88	L	–
1249+15	2.4 ± 0.3	–	1.2 ± 0.1	–	–	0.6 ± 0.1	0.5 ± 0.1	–	0.3 ± 0.1	<0.3	−1.31 ± 0.61	P	3.10
1311+22	6.3 ± 0.4	–	5.4 ± 0.3	7 ± 2	–	–	–	–	1.4 ± 0.1	1.3 ± 0.1	−1.36 ± 0.48	P	0.71
1423+39	6.6 ± 0.4	–	10.4 ± 0.6	<21	–	11.4 ± 0.8	9.5 ± 0.5	–	7.4 ± 0.4	6.8 ± 0.3	−0.81 ± 0.14	P	3.36
1446+60	3.0 ± 0.3	–	2.4 ± 0.2	–	–	1.4 ± 0.1	1.3 ± 0.1	–	0.7 ± 0.1	0.6 ± 0.1	−1.31 ± 0.26	P	1.28
1611+08	20.1 ± 1.2	–	16.6 ± 0.9	–	–	14.2 ± 0.7	14.2 ± 0.7	–	11.5 ± 0.6	10.8 ± 0.5	−0.40 ± 0.12	P	0.88

in the explored frequency range. Only for one source, 1511+25, we have two points for the SED, not allowing a parabolic fit. Thus, for this source we cannot discard the presence of a peak; however, given the clearly inverted spectrum between 1.4 and 8.3 GHz, and the upper limit at 4.8 GHz, a peak in this range is improbable. For some sources, we excluded from the fit the measurements that clearly belong to a second synchrotron component at higher or lower frequency range with respect to the fitted one. These were 1.4 GHz for 0840+34, 1129+13, 1157+22, 1348+17; 1.25 and 1.75 GHz for 1249+15; 8.5 and 9.5 GHz for 1023+55, 1125+57. The results are reported in Tables 4 and 5, including the observer's frame peak frequency, when present.

In total, 12 out of 15 BAL QSOs (80 per cent) and 10 out of 14 non-BAL QSOs (71 per cent) could be fitted with a P, and thus show hints of a peak, not suggesting a clear difference between the two samples. A selection effect, due to the requirement that sources be detected in FIRST despite the large redshift, could also have a role in selecting sources peaking in the 1–50 GHz (rest-frame) range. Nevertheless, the use of a comparison sample – selected in the same way – allows us to draw statistically significant conclusions about the differences between BAL and non-BAL QSOs.

Spectral indices

The spectral index of the synchrotron spectrum (defined here as α in the expression $S = \nu^{\alpha}$) can be a useful orientation indicator (Orr & Browne 1982). This has been used in previous works to characterize the orientation angle distribution of RL BAL QSOs (Montenegro-Montes et al. 2008; DiPompeo et al. 2011, 2012; Bruni et al. 2012) finding only a mildly preferred orientation with respect to non-BAL QSOs. We repeat here the same analysis to test the orientation scenario at high redshifts. For the calculation, we used the flux density measurements at 5 and 8.5 GHz from the JVLA, or the ones at 4.8 and 8.3 GHz from the Effelsberg-100 m dish when the previous were not available. In this way, we have an estimate as homogeneous as possible for the different sources, and consider frequencies at the right-hand side of the peak, when present. The only exceptions are the two sources presenting an inverted spectrum in the observed frequency range: BAL QSO 1511+25 and non-BAL QSO 1017+34. In this case, we are looking at the self-absorbed part of the synchrotron spectrum. The obtained values for the two samples are given in Tables 4 and 5.

Considering only the objects that do not present an inverted spectrum (i.e. $\alpha < 0$, 14 BAL and 13 non-BAL QSOs), 12/14 BAL QSOs

Downloaded from https://academic.oup.com/mnras/article-abstract/467/4/4763/2978044 by Universidad de Cantabria user on 09 July 2019

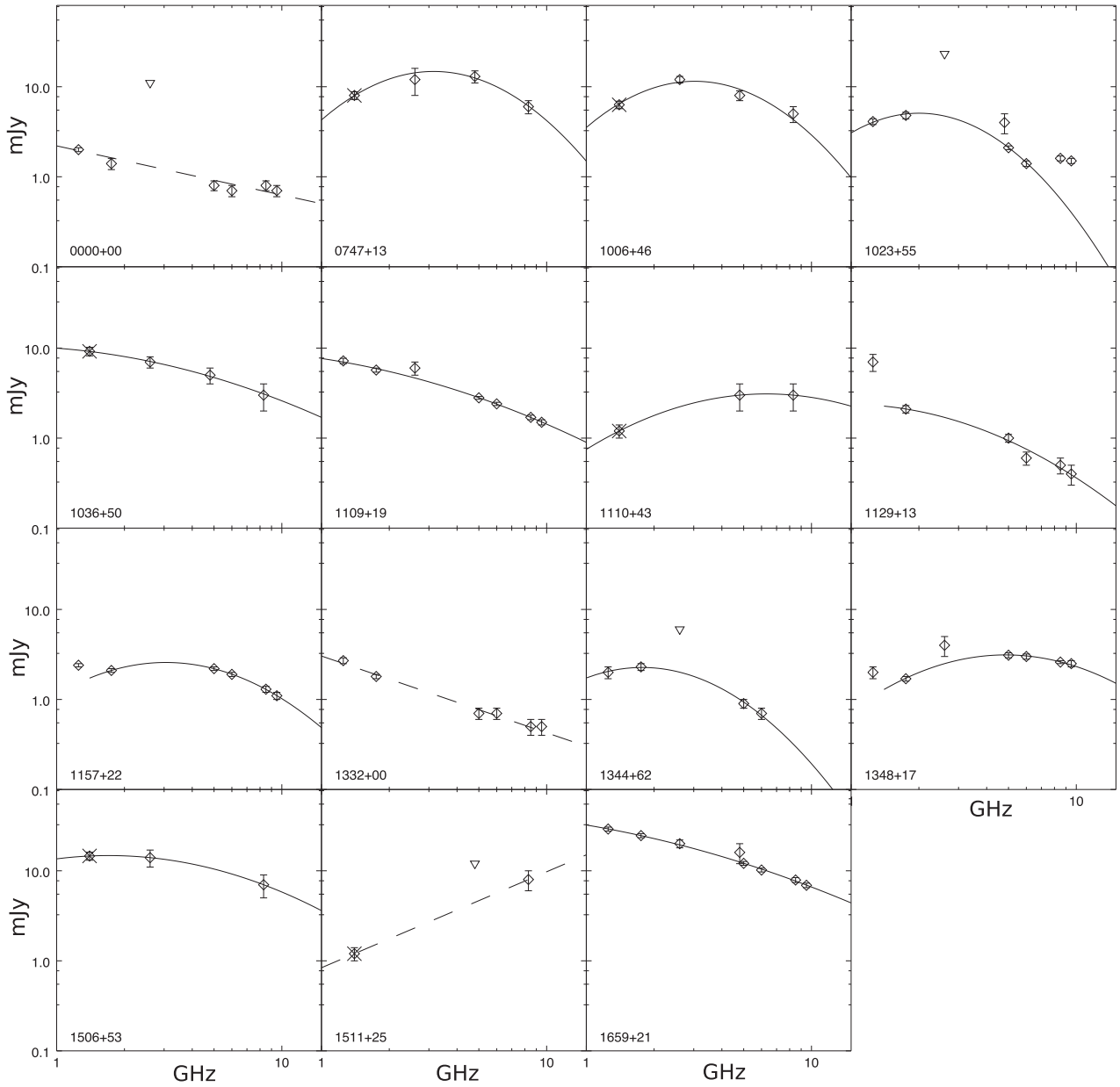

Figure 3. SEDs of the 15 high-redshift BAL QSOs studied here (*x*-axis: GHz, *y*-axis: mJy). Flux densities from the FIRST catalogue, at 1.4 GHz, are plotted as crosses. Triangles are 3σ upper limits.

(86 per cent) are steep ($\alpha < -0.5$), while 10/13 non-BAL QSOs (77 per cent) are steep. A Kolmogorov–Smirnov (K-S) test on the two spectral index distributions results in a $p = 0.40$, which does not allow us to exclude the null hypothesis that the two samples of values are drawn from the same parent distribution. Also considering the whole spectral index distributions from Tables 4 and 5 for the K-S test, we obtain a $p = 0.45$, confirming the previous result.

5 BROADBAND COLOURS OF HIGH-REDSHIFT RL BAL QSOS

The continuum emission differences between BALQSOs and non-BALQSOs can be investigated by studying the differences between their broad-band colours, since they can give an indication of the photometric spectral index. In this section, we investigate the radio-loudness, the broad-band optical (Section 5.1) and infrared (Section 5.2) colours of RL BAL QSOs in the highest redshift range for which the C IV absorption troughs are still visible in the optical spectra. For this purpose, we use all the 22 RL BAL QSOs selected in Section 2 and listed in Table 1. We compare them with normal RL QSOs in the same range of redshift ($3.6 \leq z \leq 4.8$) and detected in both SDSS DR7 and FIRST. This comparison sample consists of 99 QSOs from the SDSS DR7 QSO catalogue and it is complemented by another 14 spectroscopical confirmed QSOs selected using a 97 per cent complete selection strategy described in Tuccillo et al. (2015) and based on the use of an artificial neural network to select quasar candidates within sources without spectra in SDSS. This results in a total of 113 RL QSOs. We note that we excluded from the comparison sample five QSOs showing broad absorption in the O IV emission-line only (and not in C IV) in order to reduce any bias in the comparison between BAL and non-BAL QSOs.

Downloaded from https://academic.oup.com/mnras/article-abstract/467/4/4763/2978044 by Universidad de Cantabria user on 09 July 2019

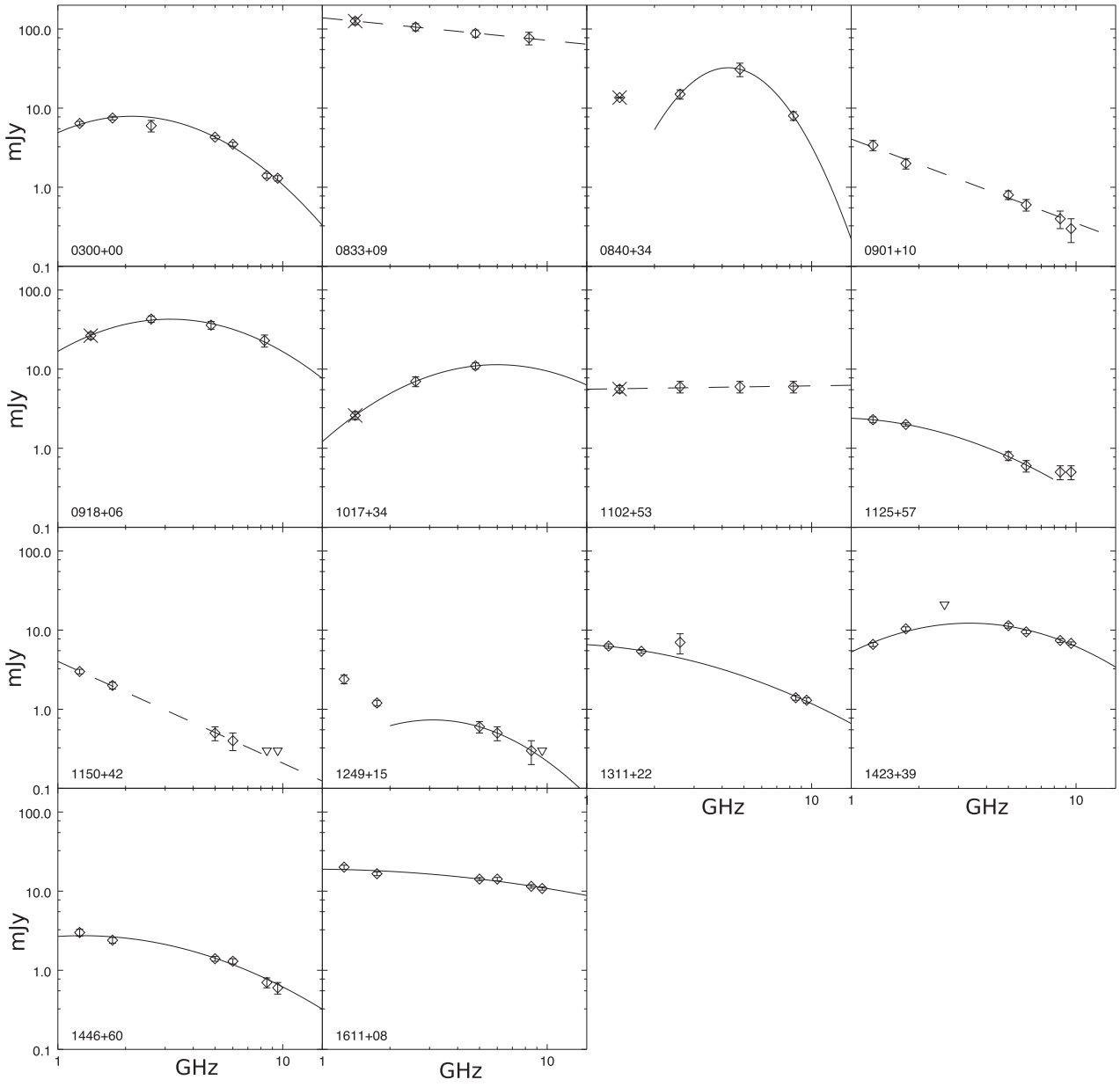

Figure 4. SEDs of the 14 comparison non-BAL QSOs (*x*-axis: GHz, *y*-axis: mJy). Flux densities from the FIRST catalogue, at 1.4 GHz, are plotted as crosses. Triangles are 3σ upper limits.

The distribution of the radio power, the *i*-magnitude and the radio-loudness, *R*, for the two samples of 22 BAL and the 113 non-BAL samples is showed in Fig. 5. All the QSOs of our sample satisfy our criteria to be detected in FIRST ($S_{1.4\,\mathrm{GHz}} > 1$ mJy) and in SDSS DR7; therefore, there is no a priori reason for which BAL QSOs should be radio and optically distributed differentlyfrom normal QSOs. In this sense, the fact that our BAL sample tends to have lower radio power is consistent with the tendency for strongly RL QSOs to lack of BAL QSOs (Becker et al. 2001; Richards et al. 2011).

5.1 Broadband optical colours

In Fig. 6, we show SDSS colour–colour diagrams of our samples of 22 BAL and 113 non-BAL QSOs. All the colours have been corrected for galactic extinction using the maps of Schlegel, Finkbeiner & Davis (1998). In the plots, the large crosses with a 1σ error bar represent the location of the mean for each of the plotted samples, respectively, red for BAL and blue for normal QSOs. BALQSOs tend to occupy redder subregions of the colour–colour space determined by the distribution of the parent population of quasars. This trend is analysed with a *t*-test to compare the means of all the SDSS colours for the BAL and non-BAL samples. In Table 6, we report only the colours for which the *t*-test rejects the null hypothesis that the colour-vectors come from normal-distributed samples having equal means, and therefore suggesting a significant difference in those values. The *t*-test is performed in the general conditions of not assuming equal variances (Behrens–Fisher problem) and the number of degrees of freedom d*f* is given by the Satterthwaite approximation.

The same trend is analysed in Figs 7 and 8, where we plot the normalized distribution of the colours for which the *t*-test gives a

Downloaded from https://academic.oup.com/mnras/article-abstract/467/4/4763/2978044 by Universidad de Cantabria user on 09 July 2019

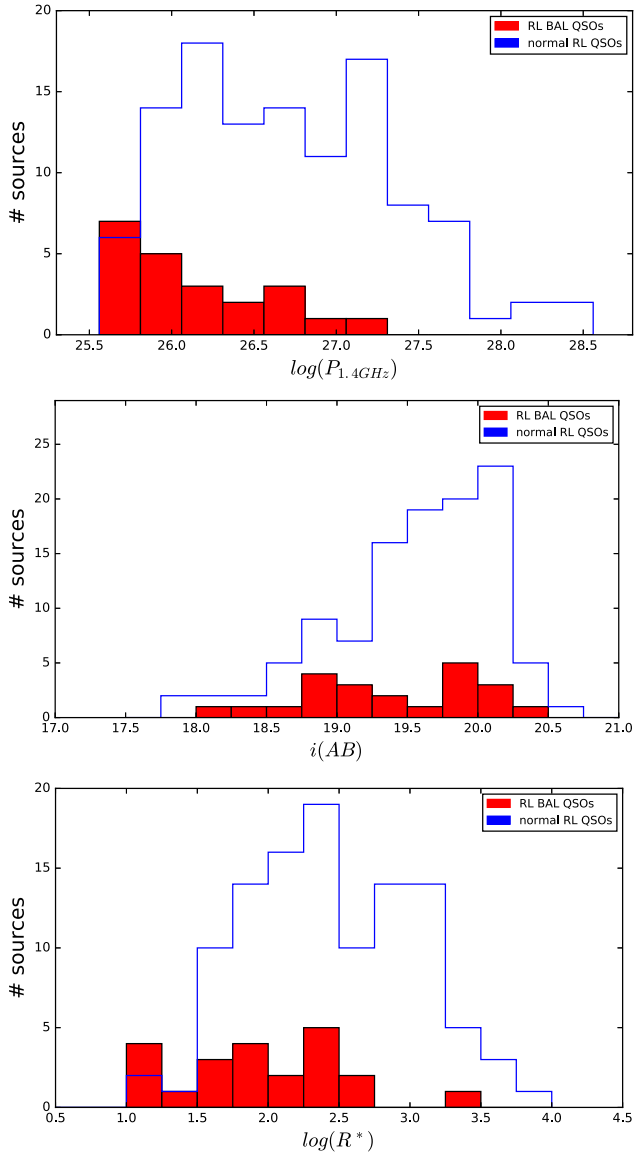

Figure 5. Distribution in radio power, i-magnitude and radio-loudness, R, for our sample of 22 $3.6 \leq z \leq 4.8$ RL BAL QSOs (red bins) and a sample of 113 normal RL QSOs (blue bins) matched in redshift. We used these samples to compare the differences between broad-band optical and NIR colours of RL BAL and non-BAL RL QSOs at high redshift. See Section 5.

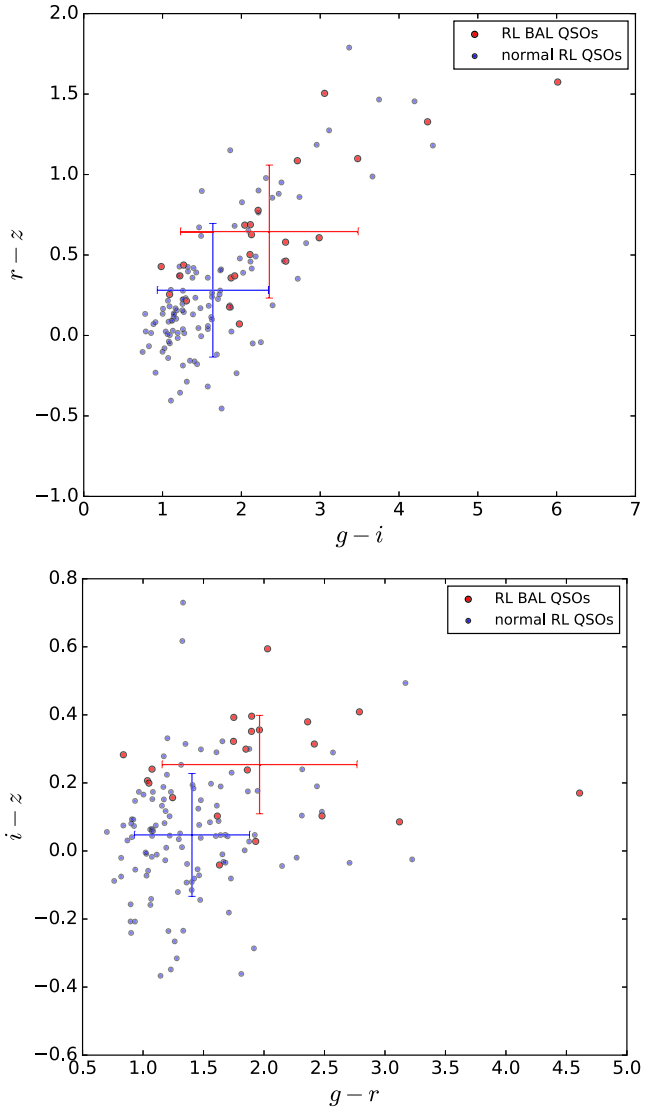

Figure 6. Two-colour diagrams presenting the SDSS colours of 22 high-redshift RL BAL (red dots) and 113 normal RL QSOs (blue dots) in the same range of redshift. We show the mean colours of the BAL sample as a red cross and the mean colours of the normal QSOs as a blue cross, both with a 1σ error bar. See Section 5.1

lower value for the statistic p, indicating a larger difference in the means of the colours for BAL and non-BAL QSOs.

5.2 Near- and mid-infrared colours

We matched our sample of 22 RL BAL QSOs and 113 normal QSOs with the LAS-DR9 UK Infrared Telescope Deep Sky Survey (UKIDSS; Lawrence et al. 2007). For each source, we searched for the nearest counterpart within 2.0 arcsec from the radio position (as given in FIRST). In fact, as shown in Wu & Jia (2010), 99.6 per cent of the SDSS QSOs having matched counterpart in UKIDSS lie within 0.5 arcsec of the SDSS positions, and the maximum radio-optical separation of the QSOs of our sample is less 1.0 arcsec. We have that 6 BAL QSOs and 49 normal QSOs lie in the footprint of UKIDSS DR9; however, only 5 BAL QSOs and 36 normal QSOs are detected in all 4 UKIDSS bands (Y, J, H, K). In Fig. 9, we show the comparison of the two samples in the $H-K$ versus $Y-J$ colour–colour space. The means of the UKIDSS colours are shown in the plot, respectively, as a red (for BAL QSOs) and a blue (for normal QSOs) cross. The t-test (see Table 7) indicates that only the means of the latter colours are statistically different from each other.

We also searched for counterparts of our sample of QSOs in the *Wide-field Infrared Survey Explorer* (*WISE*; Wright et al. 2010) most recent data release (AllWISE; Ochsenbein, Bauer & Marcout 2000) within 3.0 arcsec from the radio position. Thus, we used a slightly higher radius than the one of 2.0 arcsec used for the SDSS QSO Catalog (from the 9th DR; see Pâris et al. 2012) to cross match SDSS and *WISE*. In this case, 104 normal QSOs and all 22 BAL QSOs are detected in all four ($W1$, $W2$, $W3$, $W4$) *WISE* bands. However, we consider only the sources without image artefact contamination flags and detected with a flux signal-to-noise ratio >2 in all $W1$,$W2$ and $W3$ bands. This way, we consider two samples of 14 RL BAL QSOs and 47 normal RL BAL QSOs. Using the same methodology

Downloaded from https://academic.oup.com/mnras/article-abstract/467/4/4763/2978044 by Universidad de Cantabria user on 09 July 2019

Table 6. *t*-test on SDSS colours.

Colour (1)	Population (2)	Mean (3)	σ (4)	Median (5)	t (6)	df (7)	p ($\times 10^{-2}$) (8)
$(u-i)$	BAL	5.13	1.02	5.21	2.3	32.2	3.00
	non-BAL	4.58	1.14	4.40			
$(u-z)$	BAL	5.38	1.04	5.47	3.0	32.1	0.46
	non-BAL	4.62	1.17	4.48			
$(g-r)$	BAL	1.96	0.82	1.87	3.0	23.8	0.55
	non-BAL	1.41	0.48	1.31			
$(g-i)$	BAL	2.36	1.15	2.11	2.8	24.1	1.00
	non-BAL	1.64	0.71	1.43			
$(g-z)$	BAL	2.61	1.15	2.45	3.6	24.8	0.14
	non-BAL	1.69	0.77	1.46			
$(r-z)$	BAL	0.64	0.42	0.54	3.7	29.3	0.08
	non-BAL	0.28	0.41	0.18			
$(i-z)$	BAL	0.25	0.15	0.26	5.7	34.3	0.00
	non-BAL	0.05	0.18	0.05			

The columns give the following: (1) SDSS colour; (2) subsample considered; (3) mean of the colour; (4) standard deviation; (5) median of the colour; (6) statistic t; (7) associated degrees of freedom to the t-test; (8) the statistic p associated with the t-test, as usually, the null-hypothesis of equal mean is rejected for values <0.05.

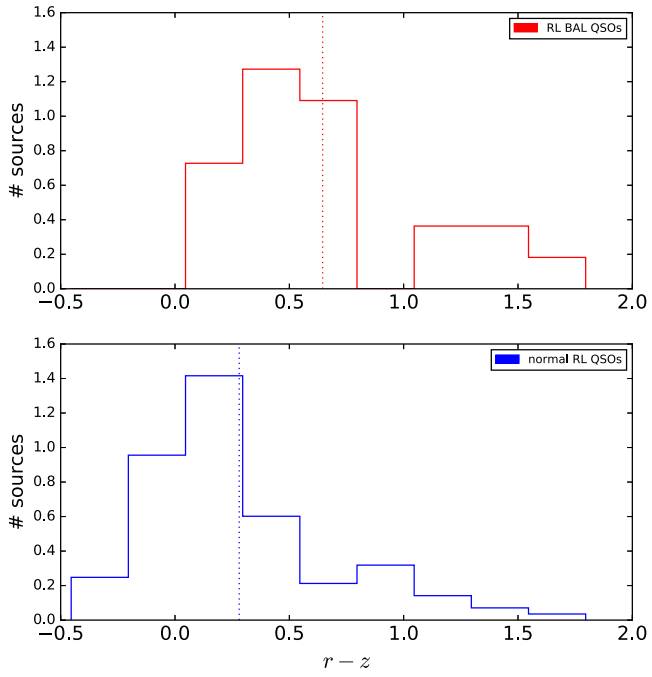

Figure 7. Comparison of the normalized distribution of the $(r-z)$ optical colours of high-redshift RL BAL and non-BAL QSOs, as discussed in Section 5.1. The mean of the BAL QSO colours is indicated by a red dashed line, while for the normal RL QSOs it is indicated by a blue dashed line.

used for the SDSS and UKIDSS colours, we compare the *WISE* colours of the two samples as shown in Fig. 10. In this case, this simple comparison of the NIR colours does not reveal differences between the two samples. The means of the colours are compared with the t-test as resumed in Table 7 and none of these means are statistically different for the two samples. Thus, we find no evidence of our high-redshift RL BAL QSOs having redder *WISE*

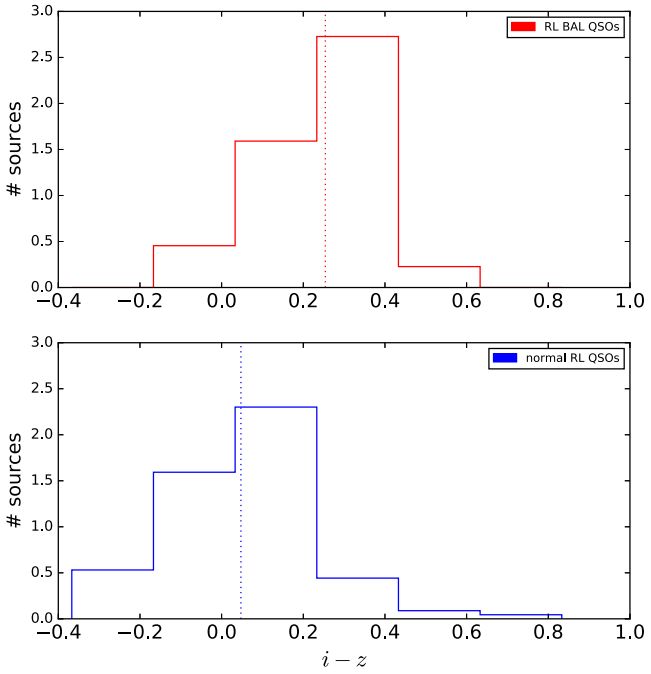

Figure 8. Comparison of the normalized distribution of the $(i-z)$ optical colours of high-redshift RL BAL and non-BAL QSOs, as discussed in Section 5.1. The mean of the BAL QSOs colours is indicated by a red dashed line, while for the normal RL QSOs is indicated by a blue dashed line.

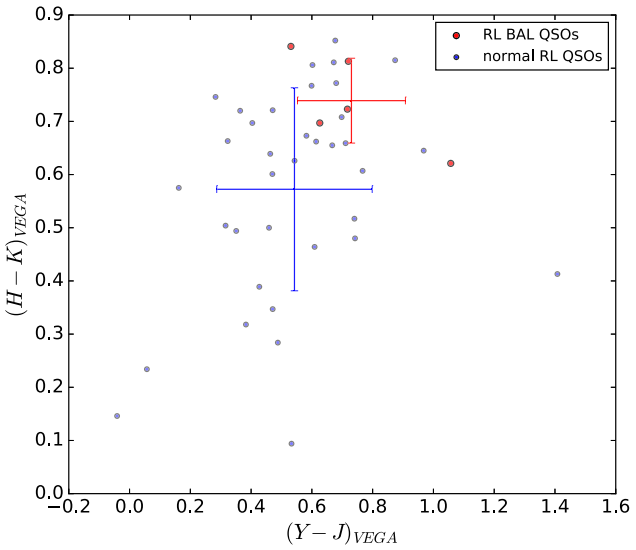

Figure 9. Comparison of the NIR UKIDSS colours for a sample of five high-z RL BAL (red dots) and 36 normal RL QSOs (blue dots) matched in redshift. The means of the colours are shown in the plot as a red cross for the BALs and blue cross for the normal QSOs, both with a 1σ error bar. See Section 5.2

colours than other optically selected RL QSOs at the same range of redshift.

6 DISCUSSION

In Section 6.1, we present the conclusions of our studies in the radio band; in Section 6.2, we present the conclusions of our investigations of optical and infrared colours of our RL BAL QSOs.

Downloaded from https://academic.oup.com/mnras/article-abstract/467/4/4763/2978044 by Universidad de Cantabria user on 09 July 2019

Table 7. *t*-test on NIR, MIR colours.

Colour (1)	Population (2)	Mean (3)	σ (4)	Median (5)	t (6)	df (7)	p ($\times 10^{-2}$) (8)
$(Y-J)$	BAL	0.73	0.18	0.72	1.90	6.1	10.56
	non-BAL	0.54	0.26	0.54			
$(H-K)$	BAL	0.74	0.18	0.72	3.2	10.44	0.83
	non-BAL	0.57	0.26	0.63			
$(W2-W1)$	BAL	−0.51	0.16	−0.46	0.5	18.9	63.82
	non-BAL	−0.49	0.14	−0.46			
$(W3-W2)$	BAL	−3.23	0.45	−3.13	0.3	23.2	78.92
	non-BAL	−3.14	0.50	−3.14			

The columns give the following: (1) near- and mid-infrared colour; (2) subsample considered; (3) mean of the colour; (4) standard deviation; (5) median of the colour; (6) statistic t; (7) associated degrees of freedom to the t-test; (8) the statistic p associated with the t-test, as usually, the null-hypothesis of equal mean is rejected for values <0.05.

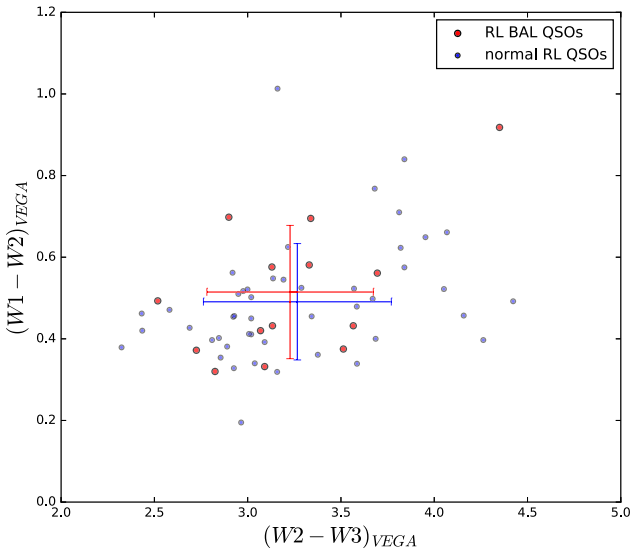

Figure 10. Two-colour diagram presenting the NIR *WISE* colours of 14 high-redshift RL BAL (red dots) and 47 normal RL QSOs (blue dots) matched in redshift. The large crosses with 1σ error bar represent the location of the mean: red for the BALs and as a blue for normal QSOs. See Section 5.2.

6.1 Radio properties

In the radio band, we studied a sample of 15 RL BAL QSOs and compared our results with the ones obtained for a well-matched sample of 14 RL non-BAL QSOs.

All objects are unresolved, even at the highest resolution observations performed with JVLA. The upper limit linear size deduced from the mean redshift of BAL and non-BAL samples is of ∼1.4 kpc, compatible with the one of radio sources in an early phase (GPS and HFP). This is consistent with the synchrotron peak frequencies found, as discussed in the next paragraph.

We reconstructed the SED of our objects between 1.25 and 9.5 GHz. The fraction of young radio sources (i.e. GPS/HFP) in the BAL and non-BAL samples are compatible within errors, thus not suggesting a particular young radio phase for BAL QSOs with respect to *normal* QSOs, even at this redshift range. A similar result was found at lower redshifts for the GPS fraction (Bruni et al. 2012).

The fact that the orientation of BAL and non-BAL QSOs does not show a significant difference is not in line with what was found in lower redshift samples (DiPompeo et al. 2011; Bruni et al. 2012). This could be an effect of the higher fraction of GPS/HFP sources present in this work, due to the considered redshift window. In fact, if outflows responsible for the BAL absorption could be later re-oriented to form the jet (Elvis 2000), young radio sources could present an outflow more likely oriented towards the polar direction, compensating for the tendency of BAL QSOs to have equatorial orientation. If verified with larger samples, this would link the jet-collimation mechanism with accretion disc outflows reorientation, favouring the hypothesis that accretion disc rotation can be at the origin of magnetic jet launching (Blandford & Payne 1982; Boccardi et al. 2016).

6.2 Broadband colours

Numerous studies on the continuum and emission-line properties of BAL QSOs spectra have been pursued in the last 25 yr, and it was soon noticed (Weymann et al. 1991) that they show redder continua than those of normal quasars. This claim has been confirmed by a number of different studies (Sprayberry & Foltz 1992; Brotherton et al. 2001; Reichard et al. 2003), and there is a general agreement on the fact that the subpopulation of LoBAL are significantly redder than HiBALs (Urrutia et al. 2009) and that HiBALs are moderately redder than quasars not showing BAL features. However, the origin of the reddening itself is still a subject of debate (see for instance Krawczyk et al. 2015) and the discussion is complicated from contrasting results in the near-infrared (Gallagher et al. 2007; DiPompeo et al. 2013). In fact, if the differences in the mean optical colours of BAL and non-BAL QSOs are consequence of a dustier environment (in agreement with the evolution scenario), they should be brighter in the infrared, where dust is seen in emission rather than in absorption.

In Section 5, we studied the SDSS optical colour distributions of our sample of 22 RL BAL QSOs and of a sample of 113 normal RL QSOs with redshift in the same range and selected using the same criteria. The colours for BAL QSOs and non-BAL QSOs indicate that BAL QSOs are redder than non-BAL QSOs, and t-tests confirm that the means of the two groups are statistically different from each other. This result cannot be due simply to absorption from the BAL troughs themselves, since the trough absorption can make the broad-band colour of BAL QSOs bluer as well as redder, depending on where the redshift of the quasar places the troughs with respect to the filters. Instead, it gives an indication of an overall flux deficit. These results confirm that BAL QSOs are redder than normal QSOs also at high redshift.

The UKIDSS colours of the subsample of 5 BAL and 36 non-BAL QSOs detected in this survey indicate that the excess is likely to be extended at the wavelength range of 0.83–2.37 μm (Hewett et al. 2006). We extend the comparison at longest wavelengths considering the 14 BAL and the 47 non-BAL QSOs detected and with reliable photometry in *WISE*. However, in this case the comparison of the colours defined from the 3.4, 4.6 and 12 μm *WISE* bands do not point to significant differences in the colours of BAL and non-BAL QSOs.

7 CONCLUSIONS

We have presented multifrequency properties of the largest sample of RL BAL QSOs detected in SDSS DR7 and having $3.6 \leq z \leq 4.8$, i.e. the highest redshift bin that allows the identification of the BAL feature with optical spectra. The sample consists of 22 RL BAL QSOs, 4 of them identified as BAL QSOs in this work for the first

Downloaded from https://academic.oup.com/mnras/article-abstract/467/4/4763/2978044 by Universidad de Cantabria user on 09 July 2019

time. We observed a fraction of them (15/22) in the radio band and we analysed optical and infrared broad-band colours of the whole sample. We can summarize the conclusions of this work as follows.

(i) All sources are unresolved, even when observed with the JVLA at 9 GHz (eight BAL versus eight non-BAL QSOs). This translates into an upper limit for the projected linear size of 1.4 kpc, compatible with the GPS/HFP classification.

(ii) We compared the peak synchrotron frequencies for the BAL and non-BAL QSO samples, not finding a predominance of GPS/HFP in the former. This does not suggest a particular younger radio phase for BAL QSOs with respect to non-BAL objects, even in this redshift range. Nevertheless, more than half of both samples can be classified as GPS/HFP, which is a larger higher fraction than the one found at lower redshift.

(iii) We derived the spectral index for the two samples and found that no statistically significant differences in orientation are present among BAL and non-BAL QSO objects. Given the high fraction of young radio sources present in this work (GPS/HFP), this could mean that BAL-producing outflows can have a preferential polar orientation in these objects, compensating the preferred equatorial orientation confirmed by different authors at lower redshifts. This would favour the hypothesis that the jet can be collimated by accretion disc driven magnetic force (Blandford & Payne 1982; Boccardi et al. 2016), since outflow orientation and newly formed jets would be connected. This should be verified on larger samples of GPS/HFP BAL QSOs.

(iv) We compare the broad-band optical and NIR colours of our sample of 22 RL BAL QSOs and of 106 normal RL QSOs matched in redshift. We find that RL BAL QSOs tend to be located, on average, in redder regions of the colour–colour space with respect to non-BAL RL QSOs. This trend is found in the optical (SDSS) and in the NIR wavelength of 0.83–2.37 μm (UKIDSS). However, we do not find significant differences in the two populations when comparing the colours at longer wavelengths, i.e. at 3.4–12 μm (*WISE*).

ACKNOWLEDGEMENTS

This work has been funded by the Spanish Ministerio de Economía y Competitividad (MINECO) under projects AYA2011-29517-C03-02 and AYA2014-58861-C3-2-P. The research leading to these results has received funding from the European Commission Seventh Framework Programme (FP/2007-2013) under grant agreement no. 283393 (RadioNet3). This work is partially based on observations with the 100-m telescope of the MPIfR (Max-Planck-Institut für Radioastronomie) at Effelsberg. We thank the Effelsberg operators for their useful help. DT also thanks the University of Wyoming for hosting his useful and nice three-month visit at their Department of Physics and Astronomy. Finally, thank you to the anonymous referee, whose constructive comments assisted in clarifying and improving complex parts of the paper.

The National Radio Astronomy Observatory is a facility of the National Science Foundation operated under cooperative agreement by Associated Universities, Inc. This research has made use of the NASA/IPAC Infrared Science Archive and NASA/IPAC Extragalactic Database (NED), which are both operated by the Jet Propulsion Laboratory, California Institute of Technology, under contract with the National Aeronautics and Space Administration. Use has been made of the SDSS Archive. The SDSS is managed by the Astrophysical Research Consortium (ARC) for the participating institutions: The University of Chicago, Fermilab, the Institute for Advanced Study, the Japan Participation Group, The John Hopkins University, Los Alamos National Laboratory, the Max-Planck-Institute for Astronomy (MPIA), the Max-Planck-Institute for Astrophysics (MPA), New Mexico State University, University of Pittsburgh, Princeton University, the United States Naval Observatory and the University of Washington.

REFERENCES

Allen J. T., Hewett P. C., Maddox N., Richards G. T., Belokurov V., 2011, MNRAS, 410, 860
Antonucci R., 1993, ARA&A, 31, 473
Baars J. W. M., Genzel R., Pauliny-Toth I. I. K., Witzel A., 1977, A&A, 61, 99
Baloković M., Smolčić V., Ivezić Ž., Zamorani G., Schinnerer E., Kelly B. C., 2012, ApJ, 759, 30
Becker R. H., Gregg M. D., Hook I. M., McMahon R. G., White R. L., Helfand D. J., 1997, ApJ, 479, L93
Becker R. H., White R. L., Gregg M. D., Brotherton M. S., Laurent-Muehleisen S. A., Arav N., 2000, ApJ, 538, 72
Becker R. H. et al., 2001, ApJS, 135, 227
Blandford R. D., Payne D. G., 1982, MNRAS, 199, 883
Boccardi B., Krichbaum T. P., Bach U., Bremer M., Zensus J. A., 2016, A&A, 588, L9
Boyle B. J., Shanks T., Croom S. M., Smith R. J., Miller L., Loaring N., Heymans C., 2000, MNRAS, 317, 1014
Brotherton M. S., van Breugel W., Smith R. J., Boyle B. J., Shanks T., Croom S. M., Miller L., Becker R. H., 1998, ApJ, 505, L7
Brotherton M. S., Tran H. D., Becker R. H., Gregg M. D., Laurent-Muehleisen S. A., White R. L., 2001, ApJ, 546, 775
Bruni G. et al., 2012, A&A, 542, A13
Bruni G., Dallacasa D., Mack K.-H., Montenegro-Montes F. M., González-Serrano J. I., Holt J., Jiménez-Luján F., 2013, A&A, 554, A94
Bruni G. et al., 2014, A&A, 569, 87
Carballo R., González-Serrano J. I., Benn C. R., Jiménez-Luján F., 2008, MNRAS, 391, 369
Dallacasa D., Stanghellini C., Centonza M., Fanti R., 2000, A&A, 363, 887
de Vries W. H., Becker R. H., White R. L., 2006, AJ, 131, 666
DiPompeo M. A., Brotherton M. S., De Breuck C., Laurent-Muehleisen S., 2011, ApJ, 743, 71
DiPompeo M. A., Brotherton M. S., De Breuck C., 2012, ApJ, 752, 6
DiPompeo M. A., Runnoe J. C., Brotherton M. S., Myers A. D., 2013, ApJ, 762, 111
Elvis M., 2000, ApJ, 545, 63
Fanti R., Fanti C., Schilizzi R. T., Spencer R. E., Nan Rendong, Parma P., van Breugel W. J. M., Venturi T., 1990, A&A, 231, 333
Fine S., Jarvis M. J., Mauch T., 2011, MNRAS, 412, 213
Gallagher S. C., Hines D. C., Blaylock M., Priddey R. S., Brandt W. N., Egami E. E., 2007, ApJ, 665, 157
Ganguly R., Brotherton M. S., Cales S., Scoggins B., Shang Z., Vestergaard M., 2007, ApJ, 665, 990
Gibson R. R. et al., 2009, ApJ, 692, 758
Gregg M. D., Becker R. H., White R. L., Helfand D. J., McMahon R. G., Hook I. M., 1996, AJ, 112, 407
Hall P. B. et al., 2002, ApJS, 141, 267
Hewett P. C., Warren S. J., Leggett S. K., Hodgkin S. T., 2006, MNRAS, 367, 454
Hopkins P. F., Elvis M., 2010, MNRAS, 401, 7
Ivezić Ž. et al., 2002, AJ, 124, 2364
Jiang L., Fan X., Ivezić Ž., Richards G. T., Schneider D. P., Strauss M. A., Kelly B. C., 2007, ApJ, 656, 680
Kellermann K. I., Sramek R., Schmidt M., Shaffer D. B., Green R., 1989, AJ, 98, 1195
Knigge C., Scaringi S., Goad M. R., Cottis C. E., 2008, MNRAS, 386, 1426
Krawczyk C. M., Richards G. T., Gallagher S. C., Leighly K. M., Hewett P. C., Ross N. P., Hall P. B., 2015, AJ, 149, 203
Lawrence A. et al., 2007, MNRAS, 379, 1599

Downloaded from https://academic.oup.com/mnras/article-abstract/467/4/4763/2978044 by Universidad de Cantabria user on 09 July 2019

Lípari S. L., Terlevich R. J., 2006, MNRAS, 368, 1001
Matthews J. H., Knigge C., Long K. S., 2017, MNRAS, in press
Menou K. et al., 2001, ApJ, 561, 645
Montenegro-Montes F. M., Mack K.-H., Vigotti M., Benn C. R., Carballo R., González-Serrano J. I., Holt J., Jiménez-Luján F., 2008, MNRAS, 388, 1853
Murray N., Chiang J., Grossman S. A., Voit G. M., 1995, ApJ, 451, 498
Ochsenbein F., Bauer P., Marcout J., 2000, A&AS, 143, 221
O'Dea C. P., 1998, PASP, 110, 493
Orr M. J. L., Browne I. W. A., 1982, MNRAS, 200, 1067
Pâris I. et al., 2012, A&A, 548, A66
Paris I. et al., 2017, A&A, 597, 79
Proga D., Stone J. M., Kallman T. R., 2000, ApJ, 543, 686
Reichard T. A. et al., 2003, AJ, 126, 2594
Richards G. T. et al., 2011, AJ, 141, 167
Rochais T. B., DiPompeo M. A., Myers A. D., Brotherton M. S., Runnoe J. C., Hall S. W., 2014, MNRAS, 444, 2498
Saikia D. J., Salter C. J., 1988, ARA&A, 26, 93
Schlegel D. J., Finkbeiner D. P., Davis M., 1998, ApJ, 500, 525
Schneider D. P. et al., 2010, AJ, 139, 2360
Silk J., Rees M. J., 1998, A&A, 331, L1
Sprayberry D., Foltz C. B., 1992, ApJ, 390, 39
Stocke J. T., Morris S. L., Weymann R. J., Foltz C. B., 1992, ApJ, 396, 487
Tolea A., Krolik J. H., Tsvetanov Z., 2002, ApJ, 578, L31
Trump J. R. et al., 2006, ApJS, 165, 1
Tuccillo D., González-Serrano J. I., Benn C. R., 2015, MNRAS, 449, 2818
Urrutia T., Becker R. H., White R. L., Glikman E., Lacy M., Hodge J., Gregg M. D., 2009, ApJ, 698, 1095
Urry C. M., Padovani P., 1995, PASP, 107, 803
Weymann R. J., Morris S. L., Foltz C. B., Hewett P. C., 1991, ApJ, 373, 23
Wright E. L. et al., 2010, AJ, 140, 1868
Wu X.-B., Jia Z., 2010, MNRAS, 406, 1583

This paper has been typeset from a TEX/LATEX file prepared by the author.

Downloaded from https://academic.oup.com/mnras/article-abstract/467/4/4763/2978044 by Universidad de Cantabria user on 09 July 2019